

Unit-cell volume change as a metric of radiation damage in crystals of macromolecules†

Raimond B. G. Ravelli,^{a*} Pascal Theveneau,^b
Sean McSweeney^b and Martin Caffrey^c

^aEuropean Molecular Biology Laboratory (EMBL), Grenoble Outstation, 6 Rue Jules Horowitz, BP 181, 38042 Grenoble CEDEX 9, France, ^bEuropean Synchrotron Radiation Facility (ESRF), 6 Rue Jules Horowitz, BP 220, 38043 Grenoble CEDEX, France, and ^cBiophysics, Department of Chemistry, The Ohio State University, 100 West 18th Avenue, Columbus, Ohio 43210, USA. E-mail: ravelli@embl-grenoble.fr

The use of third-generation synchrotron sources has led to renewed interest in the effect that ionizing radiation has on crystalline biological materials. Simple criteria have been sought to study the effects systematically. The unit-cell volume of protein crystals shows a linear increase with absorbed dose and has therefore been proposed to be such a measure. This paper demonstrates that the increase is sample dependent, and thus it might not be a useful indicator when comparing different samples. For individual samples, however, the increase can be used to quantify ambient temperature and dose-rate effects. In this study, highly absorbing cubic crystals of holoferritin have been used to accurately determine how cell volume changes with absorbed dose. The experiments show that, for this protein, a dose-rate effect exists and that trapped radicals can be mobilized at ca 180 K.

Keywords: ferritin; free radicals; glass transitions; radiation damage; dose-rate effects; macromolecules.

1. Introduction

The brightest synchrotron radiation sources create havoc with macromolecular crystals when used at design specifications. The problem of radiation damage is not only severe in studies involving enzyme kinetics and mechanisms, where cryotechniques are not always viable, but also significant for cryocooled (typically 100 K) crystals. In the course of data collection, the diffraction power of the crystal is reduced and the mosaicity and overall *B* factor increase as the sample succumbs to damage. Eventually all higher-order reflections are lost. In addition to these general effects, some highly specific structural changes can occur, such as the breaking of disulphide bonds and the loss of definition associated with carboxyl groups (Burmeister, 2000; Ravelli & McSweeney, 2000; Weik *et al.*, 2000). Both specific and non-specific effects result in loss of perfect isomorphism throughout data collection, which can hamper phasing using the multiple-wavelength anomalous dispersion (MAD) method.

If we are to make full use of bright synchrotron sources, it is imperative that we understand the damage mechanism and devise strategies for avoiding, minimizing or possibly utilizing damage. A comparison of refined structures determined with successive data sets collected on the same crystal should give the maximum amount of information as to how radiation damage affects the structure of the

system being investigated. However, these studies are not only labour intensive. They also require a lot of precious beam time.

Free radicals and other reactive species have been proposed, and in some cases have been shown (Cheng & Caffrey, 1996) to play a role in the damage mechanism. However, only those reactive species that are built up to high levels and that have relatively long lifetimes (such as $\text{RSSR}^{\cdot-}$) will be observable in the electron-density map. Most of the reactive species that are formed during irradiation (*e.g.* H^{\cdot} , OH^{\cdot} , e^{-} , $\text{Trp}^{\cdot+}$) are unlikely to be seen. Additional techniques such as electron paramagnetic resonance (EPR), mass spectrometry (MS), X-ray absorption near-edge structure (XANES) and UV/VIS spectrophotometry will be needed to establish the role played by these highly reactive species in the damage process.

Synchrotron radiation users would like to have a simple metric of the extent of radiation damage. Traditionally, mosaicity, *B* factor and $\langle I \rangle / \langle \sigma I \rangle$ have been used. However, it has been shown that specific structural radiation damage can already be visible in the electron-density maps before these parameters have changed substantially (Ravelli & McSweeney, 2000). In the latter work, it was shown that unit-cell volume increases linearly with absorbed dose for the three proteins examined. It was proposed that the rate of change (*S*) of unit-cell volume with accumulated dose ($S \equiv \Delta V / \Delta \text{dose}$) could be used as an alternative measure of radiation damage. However, the question of the reproducibility and thus the reliability of the metric was not evaluated.

In this paper, we further investigate the use of *S* as a measure of radiation damage. *S* has been found to vary widely from sample to sample. This variability exists even when uniformly sized and identically grown crystals of a single protein are used. Nonetheless, *S* can still be a useful parameter in studies of the underlying mechanism of radiation damage. Differences in *S* were observed as a function of temperature and dose rate when measurements were made using a single crystal. Some of these results suggest that trapped radicals become mobile at elevated cryotemperatures. The possibility that the observed dose-rate effect is due to beam heating is discussed.

2. Materials and methods

Several experiments were carried out using different crystals at different temperatures and dose rates. In experiment *A*, 18 different crystals were used to measure *S* at temperatures between 100 K and 180 K, one temperature point on each crystal. In experiment *B*, two crystals were used and, for each crystal, *S* was measured at two different temperatures. In experiment *C*, *S* was determined for two crystals, each at six different temperatures. Finally, in experiment *D*, the variation of *S* with dose rate was examined using one crystal.

Ferritin was used exclusively in these studies. The protein readily forms cubic crystals that allow for an accurate determination of the unit-cell volume. Ferritin is a spherical complex of protein and Fe(III). It consists of an 80 Å-diameter iron core shrouded in protein. The metal ions dramatically increase the X-ray absorption properties of ferritin and thus greatly enhance its sensitivity to radiation damage.

Horse-spleen ferritin (24-mer, 440 kDa, Fig. 1) was obtained from Sigma and used without further purification. Crystals in space group *F*432 were grown at room temperature using the vapour-diffusion hanging-drop method from 0.8 *M* ammonium sulfate, 10 *mM* cadmium sulfate and 25% *v/v* glycerol. The initial protein concentration was 13 mg ml⁻¹. Dark-red octahedral crystals of varying sizes formed within 1–5 d. Crystals were flash cooled directly from the drop.

† Presented at the 'Second International Workshop on Radiation Damage to Crystalline Biological Samples' held at Advanced Photon Source, Chicago, USA, in December 2001.

Data were collected at the undulator beamlines ID14-2 and ID14-4 of the European Synchrotron Radiation Facility (ESRF, Grenoble, France). The beam intensity was determined after calibration of the beamline counters using a 200 μm -thick calibrated windowless PIN photodiode (Hamamatsu) housed in a light-tight holder with a 30 μm aluminium window. The mirrors were slightly defocused to minimize 'hot spots' in the beam, although no beam-profiling system was available to determine beam homogeneity. Throughout each experiment, the mean incident flux through the beamline counters was recorded. The absorbed dose was calculated using the program *RADDOSE* (http://www.esrf.fr/exp_facilities/ID14-4/raddam.html) with the incident flux, the measured beam and crystal size, and the crystal content as input parameters. The ferritin crystal density and absorption coefficient were calculated to be 1.03 g cm^{-3} and 1.42 mm^{-1} , respectively [assuming 2400 Fe(III) ions in the core of the ferritin 24-mer]. There are many sources of errors in the calculation of the absorbed dose, such as the calibration of counters and assumptions about the beam profile, the beam path through the crystal and the exact crystal composition. We are actively seeking ways to reduce these errors.

Crystal temperature was regulated by an N_2 gas stream from a 600 series Oxford Cryostream. The temperature at the crystal for a nozzle-to-crystal distance of about 8 mm was determined using a thermocouple positioned in place of the crystal in the N_2 gas stream. The measured temperature was between 4 K and 9 K higher than that set at the Oxford controller. Throughout this paper, the controller-set temperature will be used.

In experiment *A*, measurements of S as a function of temperature were made on ID14-2 at an energy of 13.3 keV. 25 frames were collected on a 2×2 ADSC Quantum4 detector in five sweeps of $5 \times 1^\circ$. Each sweep started at the same oscillation angle. An exposure time of 1 s per frame was used. The time lag between sweeps was variable, though less than 1 min. Crystals were harvested from identical crystallization conditions and all had approximately the same size ($130 \times 130 \times 100 \mu\text{m}$). The crystals were slightly larger

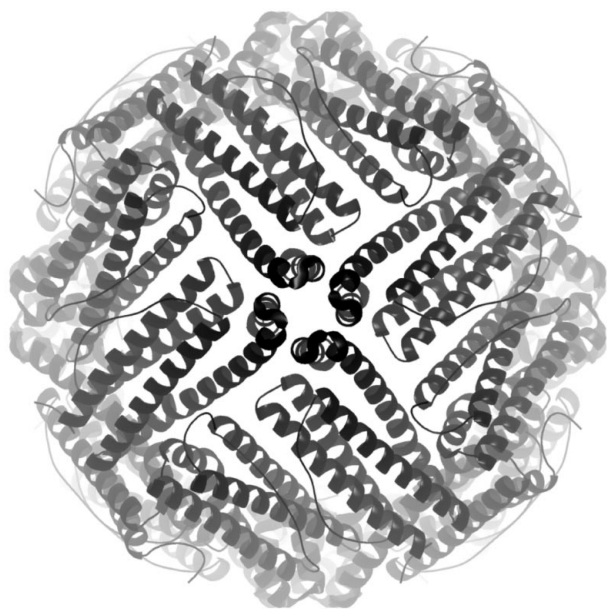


Figure 1
Ribbon diagram representation of the 24-mer of horse-spleen ferritin. An iron-mineral wall (not shown in the figure), attached to the inside of the protein coat, greatly enhances the absorbance of X-rays by the complex.

than the beam, which was slit down to $100 \times 100 \mu\text{m}$. The mean incident flux was 4×10^{11} photons s^{-1} . Two different crystals were used to determine the sample-to-sample variation in S at 100 K. The same experiments were repeated every 10 K in the heating direction from 100 K to 180 K with different crystals each time, so 18 crystals were used in total.

For experiment *B*, approximately the same conditions for crystal size, beam size and incident flux were used as for experiment *A*. S was measured with a single crystal at 100 K and 180 K. 25 frames were collected in five sweeps of $5 \times 1^\circ$ at both temperatures, with an exposure time of 1 s per frame. The first 25 frames were collected at 100 K, and the temperature was increased and stabilized to 180 K over 30 min before collecting a second series of 25 frames. The experiment was repeated with a second crystal, but this time starting at 180 K and decreasing to 100 K.

A larger crystal measuring $500 \times 500 \times 250 \mu\text{m}$ was selected in experiment *C* for the collection of 25 frames in five sweeps of $5 \times 1^\circ$ at 100 K with a beam size of $200 \times 200 \mu\text{m}$ and an incident flux of 1×10^{12} photons s^{-1} . The exposure time was 1 s per frame. Subsequently, the temperature was increased to 180 K in 20 K intervals. The same data-collection procedure was repeated on the crystal at each temperature interval. The temperature was then reset to 100 K and another set of 25 frames was collected. In total, six sets of 25 frames were collected. The temperature was raised and lowered at the rate of 300 K h^{-1} , and the average time between consecutive sets was 15 min. In order to check for reproducibility, experiment *C* was repeated on a second crystal of similar dimensions.

In experiment *D*, the effects of differences in dose rate were investigated. This experiment was performed on ID14-4 at 13.2 keV. A large crystal measuring $350 \times 350 \times 300 \mu\text{m}$ was used, and the beam-defining slits were set to provide an aperture of $300 \times 300 \mu\text{m}$. Five 1° frames were collected with a 1 s exposure time per frame and the beam attenuated 18-fold. Subsequently, the crystal was irradiated by the unattenuated beam for 5 s. The mean incident flux during irradiation was 1×10^{13} photons s^{-1} . Data were not collected in this latter period because most of the reflections were overloaded. This series of alternating measurement and burn was repeated three times.

The measurements were repeated with a beam intensity reduced by a factor of 45 (flux 2×10^{11} photons s^{-1}) and an exposure time of 225 s. Thus, the accumulated dose with the attenuated beam was the same as with the full beam. This pattern of high and low dose-rate treatments was repeated 2.5 times in total.

The diffraction data were processed using *DENZO* (Otwinowski & Minor, 1997). All crystals were prealigned to as similar an orientation as possible with the aid of the program *STRATEGY* (Ravelli *et al.*, 1997). The unit cell was refined for each frame individually, constraining the Bravais lattice to be face-centred cubic, with the crystal-detector distance fixed. Plots were made of refined cell volume on a per frame basis *versus* accumulated absorbed dose, and linear least-squares lines were fitted to determine S and the standard deviation in S (σ_S).

3. Results and discussion

Fig. 2 shows how the unit-cell volume of a single ferritin crystal increases with absorbed dose at 100 K, as determined in experiment *A*. A linear least-squares fit to the data has a slope corresponding to an S value of $0.020 \text{ \AA}^3 \text{ Gy}^{-1}$ (correlation coefficient $r = 0.9989$). Similar values for r were found for each of the crystals that were used. The value of S can vary with program and refinement procedure (Gremston, 2001), and it was therefore always determined in an identical manner. For each experiment, the crystal-to-detector

distance was refined only for the first frame and then kept fixed for all frames. The mosaicity was optimized by post-refinement and kept constant during a second round of refinement. For each frame, the unit-cell axis a was allowed to refine together with the direct beam position, crystal orientation and angular spread of the beam.

One possible explanation for the increase in unit-cell volume with absorbed dose is thermal expansion. The crystal will undoubtedly heat up as a result of exposure to the X-ray beam (Kuzay *et al.*, 2001). However, it might not return to ambient temperature in the period between successive exposures. This would result in a cumulative increase in crystal temperature. We have made measurements where the beam was off for an extended period of time during which the crystal temperature should have returned to ambient. In this case, however, the cell volume did not recover, suggesting a permanent change in structure (data not shown). This assumes that thermal hysteresis is not operative.

Fig. 3 shows S for all 18 equal-sized crystals from experiment *A*, measured at temperatures between 100 K and 180 K. The crystals were grown under identical conditions. In this temperature range, S varied from $0.009 \text{ \AA}^3 \text{ Gy}^{-1}$ to $0.022 \text{ \AA}^3 \text{ Gy}^{-1}$. The data do show sizable sample-to-sample variability, possibly masking temperature effects. We cannot identify the origins of this variability. One possibility is that the calculated accumulated dose is incorrect. This value depends on the composition of the sample through which the beam passes. The assumption is that this is constant between samples. Slight differences in size, orientation and amount of mother liquor bathing the crystal will all contribute to a real difference in the total amount of energy that is absorbed. However, simulations using *RADDOSE* show that the absorbed dose, defined as absorbed energy per mass, will vary little, since the increase in absorbed energy and mass are more or less proportional for our crystal sizes. These simulations do neglect differences in the amount of mother liquor, which might slightly change the flux reaching the crystal. We could not explain the differences in S based on mosaicity, spot shape or $\langle I \rangle / \langle \sigma I \rangle$, which can all affect the accuracy of the refined cell parameters. It is possible that the thermal history of the samples differ since this cannot be carefully controlled. This may manifest itself as differences in strain in the crystal and the vitrified surroundings, producing samples that

respond differently to the damage process that involves structural rearrangements.

It is important to note that the absolute value of S is of relevance for MAD experiments. Specifically, large values of S will add to non-isomorphism, which will lower the quality of the phases obtained from such an experiment. Based on this experience, we recommend that S be included in the criteria for selecting the best crystal for use in a MAD experiment. For example, S could be determined while collecting the first wavelength, and if it proves to be large it might be better to collect just a SAD (single-wavelength anomalous dispersion) data set.

To some degree, the sample variability noted above made it difficult to quantify the effect of temperature on S . However, when the sensitivity experiment (*C*) was performed with a single crystal, a very definite temperature dependence was apparent (Fig. 4*a*). In order to check the reproducibility of this experiment, it was repeated on a second crystal (Fig. 4*b*). The crystals showed very similar behaviour; from here on we will discuss Fig. 4*a*) only. At low temperatures (100, 120 and 140 K), the value of S was close to $0.003 \text{ \AA}^3 \text{ Gy}^{-1}$. S changed dramatically at higher temperatures, rising by a factor of four at 160 K. It then became negative at 180 K. Dropping the temperature from 180 K to 100 K restored the original value of S , recorded at the beginning of the experiment (at 100 K), although the unit-cell volume did not return to its original value on the time scale of the measurement (15 min). The thermal expansivity of the crystal is reflected in the data shown in Fig. 4, where stepwise changes in unit-cell volume occur with each change in sample temperature.

The expansion in unit-cell volume between 100 K and 140 K can be related to the linear thermal-expansion coefficient of different materials. Frauenfelder *et al.* (1987) estimated the linear thermal coefficient for myoglobin molecules to be $115 \times 10^{-6} \text{ K}^{-1}$ in the temperature range 80–300 K. This agrees with actual measurements of the unit-cell volume increase for protein crystals upon raising the temperature from 100 K to 155 K, as shown by Weik, Kryger *et al.* (2001). From Fig. 4*a*), we deduce values of $21 \times 10^{-6} \text{ K}^{-1}$ and $26 \times 10^{-6} \text{ K}^{-1}$, respectively, for the 100–120 K and the 120–140 K steps. These values are much lower than that reported by Frauen-

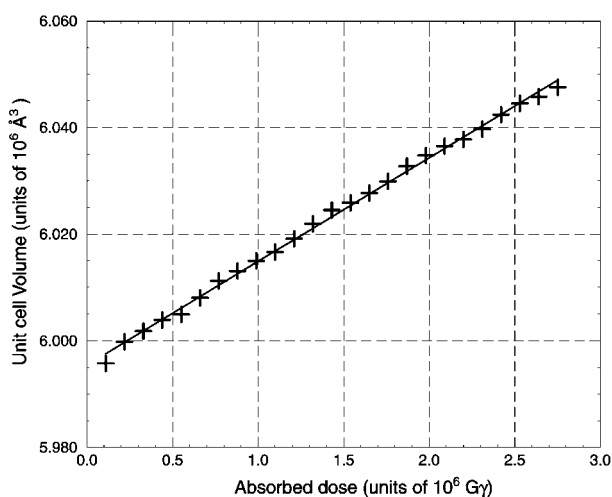


Figure 2

The dependence of ferritin unit-cell volume on accumulated dose. Each cross represents the unit-cell volume calculated from 1° images. The crystal was returned to its original orientation after every five frames. The solid line represents a linear least-squares fit. The slope of this line is called S .

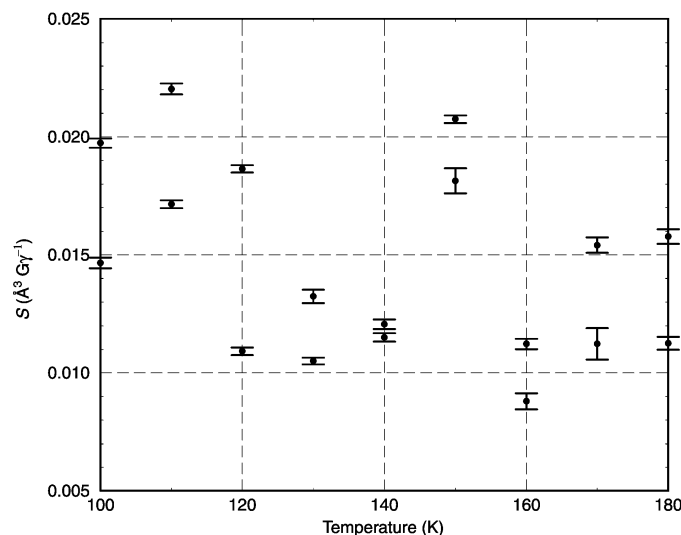


Figure 3

Thermal sensitivity of the rate of increase of unit-cell volume with accumulated dose, S , in ferritin crystals. Each datum represents a different crystal, grown under identical conditions and specially chosen for uniformity of size. The vertical bars represent the standard deviation in S , σ_S .

felder but are higher than that of pure water or pure iron [$5 \times 10^{-6} \text{ K}^{-1}$ and $12 \times 10^{-6} \text{ K}^{-1}$, respectively (Frauenfelder *et al.*, 1987)]. This low expansivity may relate to the shape and composition of the ferritin complex, where the protein only forms an envelope around a large iron-mineral core. The thermal-expansion coefficient itself is not sufficient to explain the cell-volume changes for the other temperature steps in Figs. 4(a) and 4(b) (140 K \rightarrow 160 K \rightarrow 180 K \rightarrow 100 K).

The differences in the behaviour of the unit-cell volume with accumulated dose at 160 K and 180 K compared with that at lower temperatures are probably related to the glass transition (at temperature T_g) that can occur in large solvent-filled channels in protein crystals (Weik, Kryger *et al.*, 2001). In the case of ferritin, the largest volume for the solvent is available inside the spherical protein complex. It has been shown that warming protein crystals from 100 K to 180 K results in a sharp increase in cell volume at 155 K (T_c) as a consequence of crystallization of the solvent (Weik, Kryger *et al.*, 2001). Prior to crystallization, amorphous water exhibits liquid-like

properties (Smith & Kay, 1999). In Fig. 4, a sharp increase in cell volume is observed upon changing the temperature from 140 K to 160 K and 180 K. Ice formation only became apparent in the form of ice rings in the diffraction pattern at 180 K (Fig. 5c). At 160 K, the water ring at 3.8 Å did show evidence of slight sharpening, suggesting the approach of crystallization (Fig. 5b). The higher crystallization temperature observed in this study compared with that of Weik, Kryger *et al.* (2001) may be attributable to the 25% glycerol in the mother liquor, which is known to elevate the glass transition temperature of liquids in confined channels (Weik, Kryger *et al.*, 2001). For holoferritin crystals, our data suggest that T_g and T_c are approximately 160 K and 180 K, respectively.

The value of S is about four times larger at 160 K than it is in the range 100–140 K. Surprisingly, S becomes negative at 180 K. Despite large intercrystal variations of S , we would expect to find evidence of some of these differences in Fig. 3 if the disparities are due solely to crystallization of the solvent. Since Fig. 3 does not show any such features, we believe that the high accumulated dose, as obtained for the data in Fig. 4 but not for those in Fig. 3, plays a role in the behaviour of S at 160 K and 180 K. This is in agreement with experiment B, where S was determined at 100 K and 180 K for a crystal that was heated from 100 K to 180 K and for a crystal that was cooled from 180 K to 100 K. In the latter case, the values of S were 0.0123 (3) Å³ Gy⁻¹ and 0.0123 (2) Å³ Gy⁻¹ for 180 K and 100 K, respectively, and were thus temperature independent. For the first case, where a considerable dose was accumulated before the crystal was heated, the values of S were very different: 0.0112 (1) Å³ Gy⁻¹ at 100 K and 0.0041 (3) Å³ Gy⁻¹ at 180 K.

Our hypothesis is that the increase in cell volume upon X-ray absorption is related to electrostatic repulsion between the charges that build up during an exposure. At 13 keV, the photoelectric effect is the primary source of damage and can lead to singly or multiply ionized atoms (Neutze *et al.*, 2000). The photoelectrons create a 'spur' (Singh & Singh, 1982) of radicals, most of which are immobile at 100 K. Potential energy will rise linearly with absorbed dose up to the point where spurs start to overlap. At temperatures close to the glass transition, water molecules gain rotational mobility (Fisher & Devlin, 1995). This increased mobility may facilitate potential-energy release by unit-cell expansion, resulting in an increased S at 160 K for experiment C (Fig. 4), where a large absorbed dose and thus charge accumulated before the temperature was raised. At temperatures towards T_c , translational diffusion occurs. This will not only allow water to crystallize, as observed at 180 K (Fig. 5c), but also allow radicals such as OH[•], CO₂^{•-} and solvated electrons to become mobile. Parenthetically, we note that in some EPR studies the temperature is raised to *ca* 180 K to allow radicals to recombine (Ramakrishna *et al.*, 1983). Upon charge recombination, the excess of potential energy is reduced, allowing the unit cell to expand with a lower value of S or even to shrink (Fig. 4). This is also in line with the observations of Weik, Ravelli *et al.* (2001, Fig. 4) that the unit-cell volume increases at a slower rate with increased dose for trigonal *Torpedo californica* acetylcholinesterase crystals at the crystallization temperature of the solvent (155 K), whereas it remains constant at 100 K. Clearly, additional experiments would be needed to verify our hypothesis, for example, using apoferritin, which has a much lower absorption coefficient than holoferritin. This would allow a better deconvolution of ambient-temperature-induced from radiation-damage-induced cell-volume changes.

Fig. 6 shows the result of the cell-volume *versus* absorbed-dose measurement for the dose-rate experiment (experiment D). In total, a set of 16 measurements, each consisting of five frames, were made with 'burns' imposed between each set. Burns alternated between the

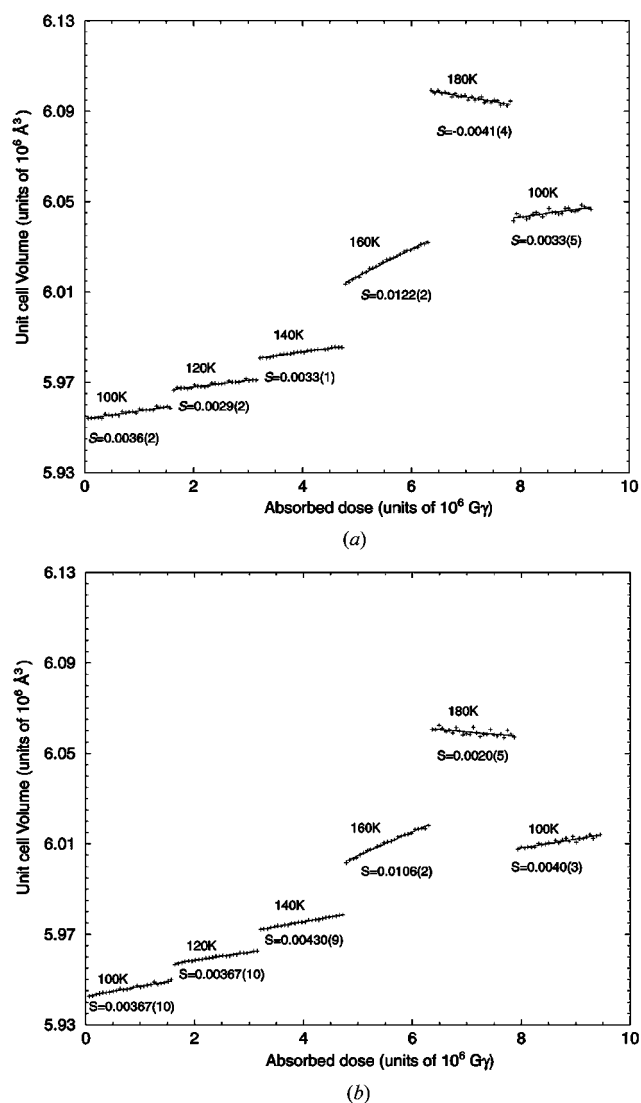


Figure 4

Thermal sensitivity of the rate of increase of unit-cell volume with accumulated dose, S , recorded using two different (a and b) large ferritin crystals. Clear temperature dependence can be observed. The meanings of the crosses and lines are as in Fig. 2.

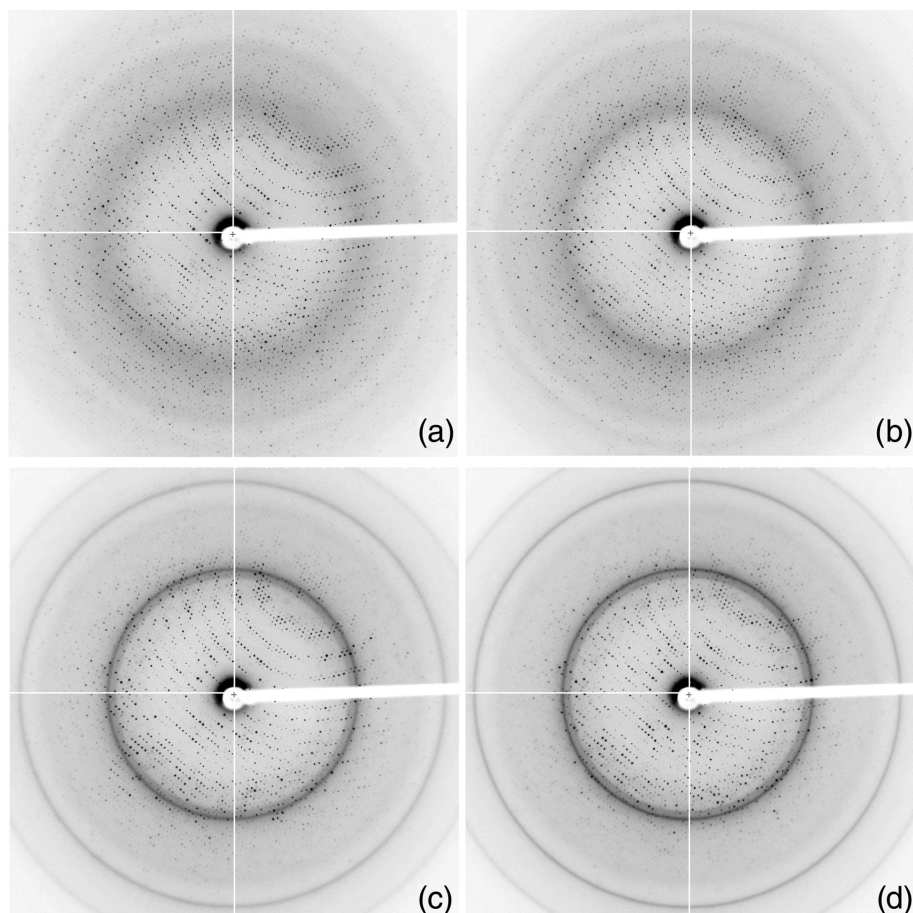


Figure 5 Diffraction patterns from a ferritin crystal recorded during the measurements reported in Fig. 4(a). The patterns shown are the first to be recorded at each temperature in the series where (a) corresponds to 100 K, (b) to 160 K and (c) to 180 K. (d) represents the first pattern at 100 K recorded upon cooling from 180 K. Irreversible ice formation is seen at 180 K.

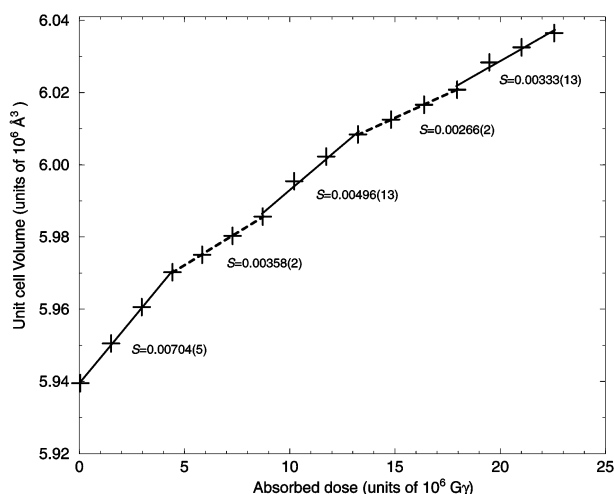


Figure 6 Dose-rate sensitivity of the rate of increase of cell volume versus accumulated dose, S . Sixteen sets consisting of five frames each were collected using a very low dose per frame. The unit-cell volume changed little within each set of five frames and was therefore averaged over these frames. Between the sets, the crystal was irradiated at different dose rates to a constant accumulated dose. The solid lines interpolate the high-dose-rate experiments; the dashed lines interpolate the low-dose-rate experiments.

full unattenuated beam (high dose rate, solid lines in Fig. 6) and the 45-fold attenuated beam (low dose rate, dashed lines in Fig. 6). However, the same accumulated dose was acquired regardless of dose rate by adjusting the exposure time. Significant differences were found for S at the low and the high dose rates. As the accumulated dose increases, the sensitivity of S to dose rate lessens, as does the overall S sensitivity to dose. This agrees with Fig. 2 of Teng & Moffat (2000), where above 1×10^7 Gy the unit-cell volume no longer shows a perfectly linear increase with absorbed dose. We speculate that this is due to spurs that begin to overlap in space at that point. However, a clear dose-rate effect can still be observed while the overall S sensitivity decreases.

To what can we attribute the observed direct dose-rate effect on S ? Following the approach introduced by Kuzay *et al.* (2001), we have calculated the maximum temperature rise in the crystal under conditions of convective cooling for the two dose rates used. Under the simplifying assumption of a lumped system where thermal gradients do not exist within the sample, the steady-state temperature rise was calculated to be 2 K and 103 K at the low and high dose rates, respectively. For comparison, the calculated maximum temperature rises for all the experiments described in this paper are given in Table 1. Even though the final steady-state temperature elevation is not insignificant for any of the crystals used, it only becomes excessive in experiment D during the high-dose-rate exposure.

Comparing the exposure time with the calculated system time constant t_{sys} (Kuzay *et al.*, 2001), it is expected that the temperature of the crystal approached the final steady-state temperature towards the end of each ‘burn’ in the dose-rate experiment. The actual temperature increase will not be constant throughout these large crystals and will differ from that calculated because of inaccuracies in the assumptions used, such as uniform beam profile and uniform heating of the crystal. However, since no ice formation was observed, the final temperature is likely to be less than 180 K. No thermal contraction was observed between the burns, where five frames were measured at low dose and low dose rates. The unit-cell volume stayed

Table 1

Calculated steady-state temperature rise and system time constant for convectively cooled crystals of ferritin exposed to an X-ray beam.

The temperature rise was calculated using equation (5) of Kuzay *et al.* (2001), assuming a lumped model for all cases, a convective heat-transfer film coefficient of $h = 100 \text{ W m}^{-2} \text{ K}^{-1}$ and $t \gg t_{\text{sys}}$, where t_{sys} is the system time constant.

Crystal of	t_{sys} (s)	$T_{\text{ss}} - T_{\infty}$ (K)	Exposure time (s)
Experiment A, Fig. 2	0.6	13	1
Experiment A, Fig. 3	0.6	13	1
Experiment C, Fig. 4	2.3	7	1
Experiment D, Fig. 6, high dose rate	2.0	103	5
Experiment D, Fig. 6, low dose rate	2.0	2	225

more or less constant for all five frames, indicating that the crystal had returned to ambient temperature before these frames were measured. This is in accordance with the model presented by Kuzay *et al.* (2001), since the time between the end of the burn and the first frame was much greater than $3t_{\text{sys}}$. From Fig. 4, it can be seen that S , when measured on one crystal, stays constant between 100 K and 140 K and only increases at 160 K. We therefore believe that the temperature could have increased to 160 K.

The predicted steady-state temperature increase of 103 K is exceptionally high because of the combination of a large beam size, high photon flux and the large absorption coefficient of the iron core in ferritin. Furthermore, an exposure time of 5 s was used to deliver the dose. This is unusually long given the flux and beam size, and it saturated most of the reflections on the detector. For the majority of the measurements currently performed at the ESRF, we do not expect beam heating to be a major problem, which is corroborated by the fact that so far we have not seen evidence for the type of behaviour exhibited in Fig. 6 using protein crystals other than ferritin. Care must be taken, however, while working with macromolecular crystals co-crystallized with high concentrations of heavy atoms in combination with a high photon flux, long exposure times and sample holders, such as the glass spatula (Yonath *et al.*, 1998), that could adversely affect the convective heat-transfer coefficient.

We would like to thank Martin Weik, David Aragao and Elspeth Garman for useful discussion and critical reading of the manuscript, and the EMBL and ESRF staff for use of the beamlines.

References

- Burmeister, W. P. (2000). *Acta Cryst.* **D56**, 328–341.
- Cheng, A. & Caffrey, M. (1996). *Biophys. J.* **70**, 2212–2222.
- Fisher, M. & Devlin, J. P. (1995). *J. Phys. Chem.* **99**, 11584–11590.
- Frauenfelder, H., Hartmann, H., Karplus, M., Kuntz, I. D. Jr, Kuriyan, J., Parak, F., Petsko, G. A., Ringe, D., Tilton, R. F. Jr, Connolly, M. L. & Max, N. (1987). *Biochemistry*, **26**, 254–261.
- Gremston, J. (2001). Part II dissertation, University of Oxford, UK.
- Kuzay, T. M., Kazmierczak, M. & Hsieh, B. J. (2001). *Acta Cryst.* **D57**, 69–81.
- Neutze, R., Wouts, R., van der Spoel, D., Weckert, E. & Hajdu, J. (2000). *Nature (London)*, **406**, 752–757.
- Otwinowski, Z. & Minor, W. (1997). *Methods in Enzymology*, edited by C. W. Carter & R. M. Sweet, Vol. 276, pp. 307–326. New York: Academic Press.
- Ramakrishna, D. N., Symons, M. C. R. & Stephenson, J. M. (1983). *J. Chem. Soc. Perkin Trans. 2*, pp. 727–730.
- Ravelli, R. B. G. & McSweeney, S. M. (2000). *Struct. Fold. Des.* **8**, 315–328.
- Ravelli, R. B. G., Sweet, R. M., Skinner, J. M., Duisenberg, A. J. M. & Kroon, J. (1997). *J. Appl. Cryst.* **30**, 551–554.
- Singh, A. & Singh, H. (1982). *Prog. Biophys. Mol. Biol.* **39**, 69–107.
- Smith, R. & Kay, B. (1999). *Nature (London)*, **398**, 788–791.
- Teng, T. & Moffat, K. (2000). *J. Synchrotron Rad.* **7**, 313–317.
- Weik, M., Kryger, G., Schreurs, A. M., Bouma, B., Silman, I., Sussman, J. L., Gros, P. & Kroon, J. (2001). *Acta Cryst.* **D57**, 566–573.
- Weik, M., Ravelli, R. B. G., Kryger, G., McSweeney, S., Raves, M. L., Harel, M., Gros, P., Silman, I., Kroon, J. & Sussman, J. L. (2000). *Proc. Natl Acad. Sci. USA*, **97**, 623–628.
- Weik, M., Ravelli, R. B. G., Silman, I., Sussman, J. L., Gros, P. & Kroon, J. (2001). *Protein Sci.* **10**, 1953–1961.
- Yonath, A., Harms, J., Hansen, H. A., Bashan, A., Schlunzen, F., Levin, I., Koelln, I., Tocilj, A., Agmon, I., Peretz, M., Bartels, H., Bennett, W. S., Krumbholz, S., Janell, D., Weinstein, S., Auerbach, T., Avila, H., Piolletti, M., Morlang, S. & Franceschi, F. (1998). *Acta Cryst.* **A54**, 945–955.